A new 3D concentration gradient maker and its application in building hydrogels with a 3D stiffness gradient

Gianni Orsi[1,2*], Marco Fagnano[1], Carmelo De Maria[1,3], Francesca Montemurro[1] and Giovanni Vozzi[1,3]

1Research Centre 'E. Piaggio', University of Pisa, Pisa, Italy

2Department of Ingegneria Civile e Industriale (DICI), University of Pisa, Pisa, Italy

3Department of Ingegneria dell'Informazione (DII), University of Pisa, Pisa, Italy

Abstract

For a deeper knowledge of phenomena at cell and tissue level, for understanding the role on bimolecular signaling and for the development of new drugs it is important to recreate in vitro environments that mimic the physiological one. Spatial gradients of soluble species guide the cells' morphogenesis, and they range in a three-dimensional (3D) environment. Gradients of mechanical properties, which have a 3D pattern, could lead cell migration and differentiation. In this work, a new 3D Concentration Gradient Maker able to generate 3D concentration gradients of soluble species was developed, which could be used for differential perfusion of scaffolds. The same device can be applied to build hydrogel matrixes with a 3D gradient of mechanical properties. Computational dynamic fluid analysis was used to develop the gradient generator; the validation of the 3D gradient of stiffness was carried out using finite elements analysis and experimental studies. The device and its application could bring improvements in studying phenomena related to cell chemotaxis and mechanotaxis, but also to differentiation in the simultaneous presence of gradients in both soluble chemical species and substrate stiffness.

Keywords bioreactors; chemotaxis; computational fluid dynamics; durotaxis; finite element analysis; polyacrylamide

1. Introduction

It has been proven that homoeotic genes responsible for cellular specialization (Driever and Nüsslein-Volhard 1988; Zákány *et al*., 2004) are activated by specific temporal and spatial gradients of soluble compounds – the so-called morphogens (Turing, 1952; Rogers and Schier 2010; Nahmad

and Lander 2011). An example of morphogen is the Sonic Hedgehog Homologue (SHH), a protein of the Hedgehog family (present only in mammals). This protein plays a key role in the differentiation of tissues making up the limbs, hands and feet, and in the organization of the nervous system (Hu and Helms, 1999; Ho and Scott, 2002; McGlinn and Tabin, 2006). For example, in the last decade it has been found that SHH plays a fundamental role in the development of the central nervous system of mice. The concentration gradient of SHH enables the correct positioning of eyes at the sides of what would become the nasal cavity. The SHH plays the same role in the human embryo (Fuccillo *et al*., 2006). Recent in vivo experiments, performed on samples of mouse and zebra fish, have shown that the presence of gradients of certain substances have a repulsive effect on the expansion of endothelial cells that will form the blood vessels. The cells stop growing in the direction characterized by an increasing concentration of Sema3A, Ephrin B2, Slit-2 and Netrin-1 (protein chemorepulsive) (Nédelec *et al*., 2012). However, other gradients promote cell growth and therefore the expansion of vascular tissue in certain directions (Neufeld et al., 1999; Lutolf *et al*., 2009). In this case, vascular cells grow when they detect an increasing concentration of vascular endothelial growth factor (VEGF) and Slit-2 (chemo-attractive protein) (Eichmann *et al*., 2005; Prasad *et al*., 2007). Slit-2 assumes the role of chemical attractant or repulser depending on cells receptor. It promotes growth when bonded to Robo-1, while it exerts opposite action if bonded to the Robo-4 (Eichmann *et al*., 2005). These changes in concentration of soluble species are necessary for the development of the vascular system, ensuring the correct presence of it throughout the human body and therefore the necessary support of nutrients for each tissue. Thus it is of interest to recreate in vitro those chemical gradients and consequently the biological phenomena driven by them. Because living organisms are complex three-dimensional (3D) structures, to fully understand the phenomena that act within it is necessary to reproduce the physiological signals in a 3D environment. Gradients of mechanical properties are also proven to influence cell migration, differentiation and activity (Zaari *et al*., 2004; Engler *et al*., 2006; Tse and Engler 2011). For example, a durotaxis (i.e. the migration guided by substrate rigidity) was discovered for fibroblasts on substrates with step-gradients in their mechanical compliance (Lo *et al*., 2000). As Engler *et al*. (2006) demonstrated, the most straightforward way to create substrates with continuous variations in mechanical compliance is to control the crosslinking density of the substrates (Zaari *et al*., 2004). This can be achieved by tuning the monomer/crosslinker ratio during polymerization. Materials with gradients in crosslinker concentrations that extend over several centimeters or millimeter could be generated easily using a gradient generator (Domingo 1990). In literature, microfluidic devices were

mainly developed to generate two-dimensional (2D) concentration gradients, which are far too simple to mimic a real physiological environment. The first 2D concentration gradient bioreactor was developed by Whitesides in 2000 (Jeon *et al*., 2000), but over the years many different 2D concentration gradient generators have appeared (Dertinger et al., 2001; Irimia *et al*., 2006; Campbell and Groisman 2007). Whitesides and his supporters, have developed other variations of this bioreactor, but always preserving the two-dimensionality of the developed concentration gradient. For example, microdevices able to create monotonic non-linear-shaped concentration gradients in the culture chamber were developed (Sun *et al*., 2008), but neither of those allowed the creation of a 3D soluble species gradient. In 2008 the Institute of Biomedical Engineering of National University of Taiwan developed another device with a geometric structure different from those already mentioned (Cheng *et al*., 2008). However, this device, while showing a different approach from Whitesides', also was unable to generate a 3D concentration gradient. The gradient maker (GM) developed in this paper preserves some characteristics of its 2D predecessors, such as a microchannels network able to generate monotonic soluble species gradients and a chamber where cells/tissues can be placed and stimulated by the chemical gradient. The flow regime in the GM chamber had to be steady and laminar but with a low Reynolds number in order to maintain a stable concentration gradient. In these flow conditions, fluid streams flow side by side, so the mixing is driven by species diffusion, with diffusion length proportional to Peclet number (Pe) (typically Pe >> 1 in liquids), and convective mixing effects are typically neglected (Perry and Green, 2008). These conditions allow prediction and control of the gradient shape with great accuracy. In this work the microfluidic device was first developed and characterized using computational fluid dynamics (CFD) in order to select the optimal topology and flow rate. Then the device was realized using 3D rapid prototyping techniques. Prototype performances were tested on a hydrogel matrix used as tissue model and placed in the GM chamber. Two dye solutions were used as 'morphogens' in order to analyse the effective formation of a 3D concentration gradient not only in the GM chamber but also inside the 'tissue'. As discussed previously, a GM can be used to fabricate a substrate with a gradient of mechanical properties: such structures were realized through the development of microfluidic networks, which can easily generate solution and surface gradients (Jiang *et al*., 2005). Here, thanks to the 3D GM, a method for fabricating 3D gradients of mechanical properties in a hydrogel was developed, which could be then perfused with a gradient of a soluble species. The 3D GM could have several applications in studying phenomena related to cell chemotaxis and durotaxis, but also for differentiation in the simultaneous presence of gradients of both soluble chemical species and

substrates stiffness. A one-dimensional gradient was usually not enough for these applications (Morishita and Iwasa, 2008, 2009).

2. Materials and methods

2.1. CFD simulations

The design of the 3D GM started with a CFD analysis. Its performances were evaluated by solving the following set of equations (equation (1)–(3)):

Navier–Stokes equation:

$$\rho(\boldsymbol{u}\cdot\nabla)\boldsymbol{u} = \nabla\cdot[-\rho\mathbf{I}+\eta(\nabla\mathbf{u}+(\nabla\mathbf{u})^{T}) \quad (1)$$

Continuity equation for incompressible fluids:

$$\nabla\cdot\mathbf{u}=0 \quad (2)$$

Fick's law (steady formulation):

$$\nabla(-\mathrm{D}\nabla\mathrm{C}) = -\mathbf{u}\cdot\nabla\mathrm{C} \quad (3)$$

where ρ, η, u, p, C and D are, respectively, fluid density, fluid viscosity, fluid velocity, pressure, species concentration, diffusion coefficient (values and measurement units are reported in Table 1). The characteristics of the velocity and concentration fields can be described through the Reynolds (Re) and Pe numbers (equation (4) and equation (5)),

$$\mathrm{Re} = \frac{\rho U d}{\mu} \quad (4)$$

$$\mathrm{Pe} = \frac{\mathrm{Ud}}{D} \quad (5)$$

where U is the mean velocity, while the characteristic fluid length d was assumed to be the hydraulic diameter, i.e.

$$\mathrm{d} = \frac{2WH}{H+W} \quad (6)$$

where W and H are the channel width and height, respectively. A three-layer 'Christmas tree' network, similar to Whitesides' solution (Jeon *et al*., 2000) and exploited in previous works (Tirella et al., 2008; Vozzi *et al*., 2010), was used to generate a linear concentration gradient through four trapezoidal inlets of the main GM chamber (Figure 1a). The structure consisted of a cubic chamber at the centre of the device (2.4 cm side), in which there were the inputs of four mixing networks placed perpendicularly. The output of the system was placed on the bottom of the x–y plane. Thus, the mixing structure had eight inputs and 16 outlets, which were inputs of GM chamber. The GM chamber had only one output (Figure 1a). The height of the mixing channels was set to 300 μm. All

pairs of input channels were set to the same average flow rate, while the chemical concentrations were equal to Cmin and Cmax, respectively. The 3D gradient concentration was obtained thanks different solute concentrations in the x–y and z planes. Tetrahedral mesh was used with average size of 0.05 mm in the inlets and 0.5 mm in the mixing chamber. In this case the flow regime was highly laminar (Re = ~7 in the inlets and Re = ~30 in the mixing chamber). A commercial CFD code, FLUENT 12.0 by Ansys Inc., (Canonsburg, PA, USA) was used to solve the 3D equations of motion.

2.2. 3D GM fabrication

The mould and the frame of the bioreactor (Figures 2 and 3) were made in acrylonitrile butadiene styrene (ABS) using a rapid prototyping system (Dimension Elite Stratasys®, Edina, Minnesota, USA). The architecture of mould was designed using Solidworks® software (Dassault Systèmes, Vélizy, France), exported in STereoLithography (STL) format and then imported in the control software of the Stratasys machine. However we found that we could not directly build the mould for the microfluidics channels (Figure 2) with this technique because of the finite resolution of the 3D printer. The natural roughness of the 3D printer (~250 μm, Figure 2g) was comparable to our microchannels size (300 μm) and thus could lead to non-tight sealing and unwanted leakage from the microchannels. In order to avoid this, we made the microchannels mould by casting the PolyDiMethylSiloxane (PDMS) (Sylgard® 184; Dow Corning, MIdland, MI, USA) onto a silicon wafer, where negative 300 μm structures of the microchannels were previously made using the soft-lithography technique (Figure 2b). The negative photoresist SU-8 (MicroChem, Newton, MA, USA) was spin-coated on the wafer, baked to drive off the solvent and exposed to UV rays (CL-1000 Ultraviolet Crosslinker UVP Upland, California, USA) through a mask. The mask was created using CorelDraw 9.0 (Corel Corporation, Ottawa, Canada) and printed on a transparency using a commercial Linotronic-Hercules 3300 dpi high-resolution line printer (Brakensiek, Dortmund, Germany). The exposed photoresist was baked again to complete polymerization, and then developed (SU-8 developer; MicroChem) to dissolve un-irradiated material (Vozzi *et al*., 2003). A 3D printed base plus a Plexiglas cover (Figure 2c) were placed over the silicon wafers in order to act as a mould for the PDMS. The PDMS was prepared by mixing in a weight ratio of 10:1 monomer and catalyst. The PDMS solution was degassed under vacuum, cast in this mould and then cured overnight at 60 °C. These parts were then placed in a 3D printed support as shown in Figure 2e,f. The GM main core was also made in PDMS, prepared as previously described. Silicone tubes with an inner diameter of 2 mm and external diameter of 4 mm were placed in the GM inlet positions before casting PDMS in the mould. After PDMS casting the mould was cured for 7 h at 70 °C. With

this procedure, the PDMS was not completely stuck to the PDMS positive parts of the mould, so it was possible to extract the GM core from the mould without destroying either the mould or the GM core. As may be seen in Figure 2g the GM surface obtained in this manner was very flat. To ensure a perfect seal a purpose-developed locking system (Figure 3a) was designed and produced. It was composed of a plastic frame made of ABS and two 6 mm Plexiglas layers, in order to maintain a free visual path to observe what happens inside the chamber and the microchannels. To ensure a tight seal of all parts eight plastic O-rings were placed between the cylindrical inserts present on the external surfaces of the frame. The deformability of PDMS established a tight seal after compression. The assembled reactor with the concentration gradient formation inside is shown in Figure 3b,c and the different concentration patterns that could be obtained in the GM are shown in Figure 3d–g. A set of peristaltic pumps (IPC, ISMATEC, Wertheim, Germany) was used for system perfusion. The gradient maker prototype provided an 8 ml chamber in order that hydrogel samples could be sliced to perform mechanical tests on different areas. External gradient length depends on the application, varying from ~150 μm in cell development (Lander, 2007) to several millimetres for complex embryo development (i.e. Xenopus) (Williams *et al*., 2004). The novelty of the developed system is that it could be easily downscaled in order to reproduce different gradient length.

2.3. Polyacrylamide mechanical characterization as function of bisacrylamide concentration

Polyacrylamide (PAAM) was chosen as a template hydrogel because of the ease in tuning its mechanical properties by just changing the acrylamide (AAM)/bisacrylamide (BIS) ratio (monomer/crosslinker ratio). Compressive mechanical tests were performed imposing different strain rates using the twin column ProLine Z005 testing machine (Zwick-Roell, Ulm, Germany) equipped with a10 N (0.04 N sensitivity) load cell at room temperature. The PAAM samples were tested partly immersed in water to preserve their hydration. Each test was performed using a starting configuration with the upper plate placed near the sample but not in contact, in similar manner as Tirella *et al*. (2013) did in their work, which necessary to guarantee known initial conditions. Quasi-static stress–strain time series were collected compressing samples (n = 3) up to 10% deformation using two different strain rates (0.0125/min and 0.0063/min), in order to evaluate the Young modulus dependency from strain rate. The Young modulus of the sample tested was evaluated as the slope of first linear part of the stress–strain diagram. The strain rate was chosen on the basis of previous works on hydrogels (Orsi *et al*., 2012). However, the strain rate was found not to influence measured mechanical properties (as shown in Figure 4), so all tests were performed at the higher strain rate. In order to have a correct mechanical characterization of PAAM samples,

it was important that they presented a flat and uniform surface. When the PAAM was cast in a 24-well plate the formation of a meniscus on the sample was observed, which resulted from the combined effect of PAAM volume retirement during gelation and capillary forces. The meniscus induced an unreliable estimation on Young modulus, greatly increasing the standard deviation of the measurements up to 20% of the mean. In order to obtain reliable uniform samples a custom-made mould was developed, which is shown in Figure 4. The mould was based on the 24-well plates, and it comprised three parts: (1) a flat base, where only 3 mm holes for assembling with nuts and bolts were drilled; (2) a middle part where, apart from the assembling holes, 24 holes with a diameter of 13 mm were drilled, these being the PAAM sample locations; (3) a top part, identical to the previous one, which could be detached just after the polymerization, to cut the top part of the sample. After the PAAM polymerization and the detachment of the top part, the top part of the samples that protruded from the middle part was cut with a sharp microtome blade. In this way smooth surfaces was also obtained in the top part of the samples, thus eliminating the meniscus problem. In this way 13 × 8 mm uniform samples were obtained. The PAAM gel was made from 8% (w/v) AAM and 0.04% up to 0.6% (w/v) BIS. As per the manufacturer's datasheet (Bio-Rad, Hercules, California, USA) 1/100 of ammonium persulphate (AP, initiator) and 1/1000 of tetramethylethylenediamine (TEMED, catalyst) were added to the solution, in order to obtain PAAM gelation. Free radical polyacrylamide polymerization was used because visible gelation occurs in 15–20 min and polymerization is essentially complete in ~90 min, whereas in photochemical polymerization visible gelation and complete polymerization take much longer. The 3D diffusion time for half-chamber length (1 cm) is L2/6D ~ 4.5 h (where L is the characteristic chamber length and U is the average velocity; Crank 1979), which is lower than the photopolymerization time, but higher than that for chemical polymerization. Photo-crosslinking could be combined in future with the 3D concentration generator, in order to achieve more complex structures, but there is a need to carefully choose the monomer, the initiator and the light source.

2.4. Realization and characterization of a hydrogel with a 3D gradient of mechanical properties

An 8% w/v solution of AAM with, respectively, 0.04% w/v or 0.6% w/v of BIS flowed from the inlets, so that a BIS concentration gradient was set in the main chamber. In addition the initiator AP was perfused from the inlets. When a steady-state flow was reached an injection of TEMED from a hole on the top in the main chamber quickly polymerized the hydrogel into the main chamber. The 3D controlled distribution of BIS into the gradient chamber led to the development of a gradient of mechanical properties in the polymerized hydrogel. Reaction time (first gelation observed, in

minutes) is significantly higher than BIS diffusion time (several hours), so it could reasonably be assumed that the distribution of BIS remained the same as the applied gradient even during the polymerization. The diffusivity of BIS (D ~10–9 m2/s) (Pascal et al., 1993) is slightly higher than that of VEGF and SHH (D ~1.5 × 10–10 m2/s) (Nauman *et al*., 2007). However, it is possible to tune the chamber flow rate in order to bring the chamber Pe to the same that of BIS, so the diffusion pattern remains the same. For these reasons BIS could be also used as a reliable diffusion model for a growth factor. The main 'cube' was cut in 3 × 3 × 4 small samples, in order to obtain a good estimation of the distribution of the mechanical properties in the 3D environment. The 'cube' was cut using the tools depicted in Figure 5, in order to ensure a uniform and repeatable slicing. Briefly the cube was placed in the bigger mould and then cut into four slices with a histological sharp blade. Each one of the four slices was then placed in the second mould and then sliced in nine equal pieces. The choice of critical size resulted from the detection limit of load cell. Each sample was subjected to a compression test using the previously described Zwick-Roell Z005 testing machine. The Young modulus of the tested sample was determined by evaluating the slope of first linear part of the stress–strain diagram, as above.

2.5. Mechanical simulation of mechanical gradient structure

There was a challenge in comparing experimental vs. simulated data. Classical fluid dynamics investigation tools such as laser-induced fluorescence (Fu *et al*., 2006) or 3D laser Doppler anemometry (Galletti *et al*., 2009) could only evaluate the fluid behaviour in the inner device. However, a direct comparison between the measured Young moduli of the sliced cube parts and the simulated concentration profile into the bioreactor, using finite element analysis (FEA) was desired. In order to do this, a fluid and mass transfer simulation with Ansys FLUENT was performed. The final BIS concentration profile was then exported by taking into account the spatial node position and value. This concentration profile was 'sliced' in 3× 3 × 4 parts, matching the experimental slicing of the PAAM cube. This concentration profile was then transformed in the Young modulus profile by using the inverse function of measured Young modulus vs. BIS (Figure 4c), and imported in COMSOL (Stockolm, Sweden) multiphysics as the point-wise elastic modulus of the sample. The mesh size of the 250 k tetrahedral elements was 0.3 mm. Each cubic sample was subjected to 1% compression in the same direction of the experimental slices deformation, by assuming elastic behaviour (shown in stress–strain experimental data). The boundary conditions of the sample were a fixed constraint on the bottom face of the sample, while the 1% compression was imposed on the opposite face. Then the reaction forces in the top boundary were evaluated by

integrating the point-wise force contribution, as the transducer does in the real experiment. The simulated Young modulus was evaluated by the formula $E = F/A\varepsilon$, where F was the calculated reaction force, A was the nominal undeformed sample section and ε (equal to 0.01) was the imposed deformation. The elastic moduli estimated with FEA were then compared with experimental moduli.

3. Results

The aim of this study was to fabricate and to characterize a 3D GM, with a design driven by CFD simulation, and whose application could span from the generation of 3D morphogen gradients to fabrication of 3D stiffness graded materials. As indicated earlier, different concentration patterns can be obtained in the GM (Figure 3d–g). However there was a limited range of flow rates that allowed the formation of the concentration gradient. For example, if flow rate was 20 times bigger or lower than the one reported in Table 1, there was no marked gradient concentration profile in the GM chamber. Low flow rate enhances the effect of diffusive mixing, so the average length in order to have complete mixing owing to diffusion in a 3D environment (equal to UL2/6D; Crank 1979) is comparable to chamber length. High flow rate instead led to fast convective mixing in the main chamber. By increasing Re, fluid inertial effects on fluid streams became bigger and there was a fast mixing of liquid streams owing to convective effects. The mass exchange between fluid streams in this case were not mainly diffusion driven. In water-based systems Pe is usually $> > 1$, and so convective mixing, when it occurs, largely predominates compared with diffusive mixing. The results of the mechanical testing are shown in Figure 5. It can be seen that there is there is a well-developed 3D gradient of mechanical properties. An evident gradient of Young modulus could be found in z and y directions, following the 3D concentration pattern of the flow, but a less steep variation could also be found in x direction (especially in slice $z = 4$). A scaffold made with this variation of stiffness could be used to promote differential proliferation in a 3D environment, previously demonstrated in 2D (Zaari *et al*., 2004). The comparison between theoretical mechanical properties distribution and the experimental one is shown in Figure 6. Experimental and simulated values are quite close in the upper part of the GM (Figure 6c,d), with an Root Mean Squared (RMS) error of ~2.5 kPa, while the lower part shows larger discrepancies (data not shown). The differences in the upper part, near the microchannels outlet, could result be an effect of the peristaltic pump that was used as supply. During pulsed flow the fluid streams reach the GM chamber with some delays, and it could bring unexpected mixing behaviour within the microchannel networks. In the literature, it has been described that pulsed flow could enhance local mixing in T-shaped microfluidic branches (Glasgow *et al*., 2004). Those structures represented the mixing sites of our microchannels

network (Orsi et al., 2013), so the simulated mixing features could be slightly different from the experimental ones. In addition, an expected diffusion of L = (6Dt)1/2 ~ 6 mm was expected to take place during the 2 h of PAAM polymerization, further smoothing the gradient This diffusion length is, however, overestimated because during the polymerization the diffusion properties of crosslinker decrease over time. While the differences between modelled and experimental stiffness in the upper two slices were acceptable, the lower part of the device showed larger differences (Figure 6). This probably occurred as a result of boundary effects near the outlet, which caused unexpected flow distortions because of the dramatic decrease of flow speed, so smoothing the gradient in an unacceptable manner.

4. Conclusion

This paper has presented a new generation of bioreactor used to fabricate hydrogel matrixes with a 3D gradient of stiffness. Although there are some discrepancies between theoretical and experimental results, for which future robustness analysis will be performed, this bioreactor can also be used for perfusion of 3D cell scaffolds with a stable gradient of chemical species (e.g. growth factor to induce cell differentiation directly into the scaffold). The idea is to seed the cells in a 3D stiffness gradient scaffolds and stimulate them with a 3D concentration gradient in order to combine mechanical and biochemical stimuli to drive tissue development.

References

Campbell K, Groisman A. 2007; Generation of complex concentration profiles in microchannels in a logarithmically small number of steps. Lab Chip 7: 264–272.

Cheng J-Y, Yen M-H, Kuo C-T, et al. 2008; A transparent cell culture microchamber with a variably controlled concentration gradient generator and flow field rectifier. Bio-microfluidics 2: 24105.

Crank J. 1979; The Mathematics of Diffusion. Oxford Science Publications: Oxford, UK.

Dertinger SKW, Chiu DT, Jeon NL, et al. 2001; Generation of gradients having complex shapes using microfluidic networks. Society 73: 1240–1246.

Domingo A. 1990; Exponential gradient maker using a disposable syringe. Anal Biochem 189: 88–90.

Driever W, Nüsslein-Volhard C. 1988; A gradient of bicoid protein in Drosophila

embryos. Cell 54: 95–104.

Eichmann A, Le Noble F, Autiero M, *et al*. 2005; Guidance of vascular and neural network formation. Curr Opin Neurobiol 15: 108–115.

Engler AJ, Sen S, Sweeney HL, *et al*. 2006; Matrix elasticity directs stem cell lineage specification. Cell 126: 677–689.

Fu J-L, Fang Q, Zhang T, et al. 2006; Laser induced fluorescence detection system for microfluidic chips based on an orthogonal optical arrangement. Anal Chem 78: 3827–3834.

Fuccillo M, Joyner AL, Fishell G, 2006; Morphogen to mitogen: the multiple roles of hedgehog signalling in vertebrate neural development. Nature Rev Neurosci 7: 772–783.

Galletti C, Pintus S, Brunazzi E. 2009; Effect of shaft eccentricity and impeller blade thickness on the vortices features in an unbaffled vessel. Chem Eng Res Design 87: 391–400.

Glasgow I, Lieber S, Aubry N. 2004; Parameters influencing pulsed flow mixing in microchannels. Anal Chem 76: 4825–4832.

Ho KS, Scott MP. 2002; Sonic hedgehog in the nervous system: functions, modifications and mechanisms. Curr Opinion Neurobiol 12: 57–63.

Hu D, Helms J. 1999; The role of sonic hedgehog in normal and abnormal craniofacial morphogenesis. Development 126: 4873–4884.

Irimia D, Geba DA, Toner M, 2006; Universal microfluidic gradient generator. Society 78: 3472–3477.

Jeon NL, Dertinger SKW, Chiu DT, et al. 2000; Generation of solution and surface gradients using microfluidic systems. Processing 15: 8311–8316.

Jiang X, Xu Q, Dertinger SKW, et al. 2005; A general method for patterning gradients of biomolecules on surfaces using microfluidic networks. Society 77: 2338–2347.

Lander AD. 2007; Morpheus unbound: reimagining the morphogen gradient. Cell 128: 245–256.

Lo CM, Wang HB, Dembo M, et al. 2000; Cell movement is guided by the rigidity of the substrate. Biophys J 79: 144–152.

Lutolf MP, Gilbert PM, Blau HM. 2009; Designing materials to direct stem-cell fate. Nature 462: 433–441.

McGlinn E, Tabin CJ. 2006; Mechanistic insight into how Shh patterns the vertebrate limb. Curr Opin Genet Dev 16: 426–432.

Morishita Y, Iwasa Y. 2008; Optimal placement of multiple morphogen sources. Phys Rev E 77: 041909.

Morishita Y, Iwasa Y. 2009; Accuracy of positional information provided by multiple morphogen gradients with correlated noise. Phys Rev E 79: 061905.

Nahmad M, Lander AD. 2011; Spatiotemporal mechanisms of morphogen gradient interpretation. Curr Opin Genet Dev 21: 726–731. Nauman JV, Campbell PG, Lanni F, et al. 2007; Diffusion of insulin like growth factor-I and ribonuclease through fibrin gels. Biophysical journal 92: 4444–4450.

Nédelec S, Peljto M, Shi P, et al. 2012; Concentration-dependent requirement for local protein synthesis in motor neuron subtype-specific response to axon guidance cues. J Neurosci 32: 1496–1506.

Neufeld G, Cohen T, Gengrinovitch S, et al. 1999; Vascular endothelial growth factor (VEGF) and its receptors. FASEB J 13: 9–22.

Orsi G, Carta V, Vozzi G. 2012; Hydrogels with 3D gradient of mechanical properties. In Hydrogels: Synthesis, Characterization and Applications, Câmara FV, Ferreira LJ (eds). Nova Publishers: New York, NY.

Orsi G, Roudgar M, Brunazzi E, et al. 2013; Water–ethanol mixing in T-shaped microdevices. Chem Eng Sci 95: 174–183.

Pascal P, Duhamel J, Wang Y, et al. 1993; Fluorescence depolarization and quenching studies of acenaphthalene-labelled poly(acrylamide) in water. Polymer 34: 1134 1140.

Perry RH, Green DW. 2008; In Perry's Chemical Engineers' Handbook, RH Perry, DW Green, JO Maloney (eds). McGraw Hill: New York City, NY, USA.

Prasad A, Qamri Z, Wu J, et al. 2007; Slit-2/ Robo-1 modulates the CXCL12/CXCR4-induced chemotaxis of T cells. J Leukoc Biol 82: 465–476. Rogers KW, Schier AF. 2010; Morphogen gradients: from generation to interpretation. Annu Rev Cell Dev Biol 27: 377–407. Sun K, Wang Z, Jiang X. 2008; Modular microfluidics for gradient generation. Lab on a Chip 8(9): 1536–1543.

Tirella A, Marano M, Vozzi F, et al. 2008; A microfluidic gradient maker for toxicity testing of bupivacaine and lidocaine. Toxicol In Vitro 22: 1957–1964.

Tirella A, Mattei G, Ahluwalia A. 2013; Strain rate viscoelastic analysis of soft and highly hydrated biomaterials. J Biomed Mater Res A.

Tse JR, Engler AJ. 2011; Stiffness gradients mimicking in vivo tissue variation regulate mesenchymal stem cell fate. PLoS One 6: e15978. Turing AM. 1952; The chemical basis of morphogenesis. Phil Trans R Soc B Biol Sci 237: 37–72.

Vozzi G, Flaim C, Ahluwalia A, et al. 2003; Fabrication of PLGA scaffolds using soft lithography and microsyringe deposition. Biomaterials 24: 2533–2540.

Vozzi G, Mazzei D, Tirella A, et al. 2010; Finite element modelling and design of a concentration gradient generating bioreactor: application to biological pattern formation and toxicology. Toxicol In Vitro 24: 1828–1837.

Williams PH, Hagemann A, GonzálezGaitán M, et al. 2004; Visualizing longrange movement of the morphogen Xnr2 in the Xenopus EMBRYO. Curr Biol 14: 1916–1923.

Zaari N, Rajagopalan P, Kim SK, et al. 2004; Photopolymerization in microfluidic gradient generators: microscale control of substrate compliance to manipulate cell response. Adv Mater 16: 2133–2137.

Zákány J, Kmita M, Duboule D. 2004; A dual role for Hox genes in limb anterior–posterior asymmetry. Science 304: 1669–1672.

Tables

Parmeters	Value	Symbol
Fluid density	103 kg/m^3	ρ
Fluid viscosity	10^{-3} Pa/s	η
Diffusion coefficient	10^{-9} m^2/s	D
Concentration input	10–3 mol/m3	C_0
Flow rate (inflow)	170 × 10–6 l/min	Q

Table of figures

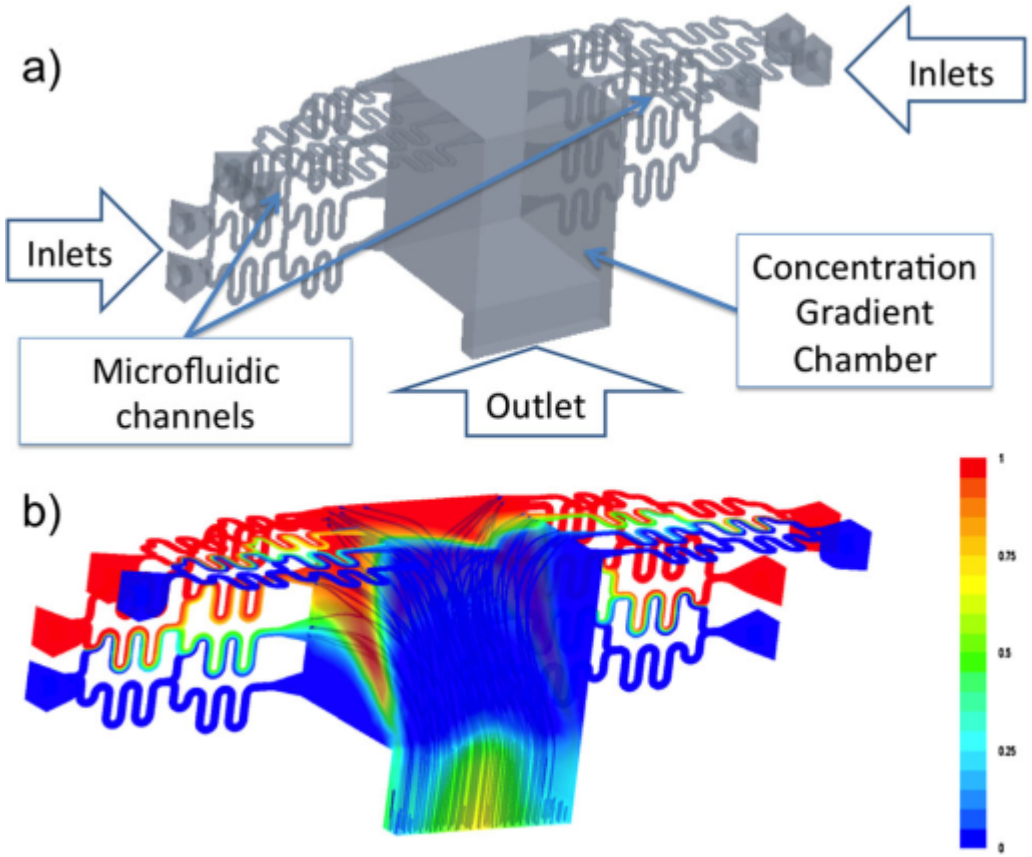

Figure 1. Concept of the three-dimensional (3D) gradient maker (GM): (a) wireframe and functional parts of the 3D GM; (b) computational fluid dynamics simulation of the 3D GM, with normalized concentration pattern (in colour scale) and fluid streamlines (blue lines inside).

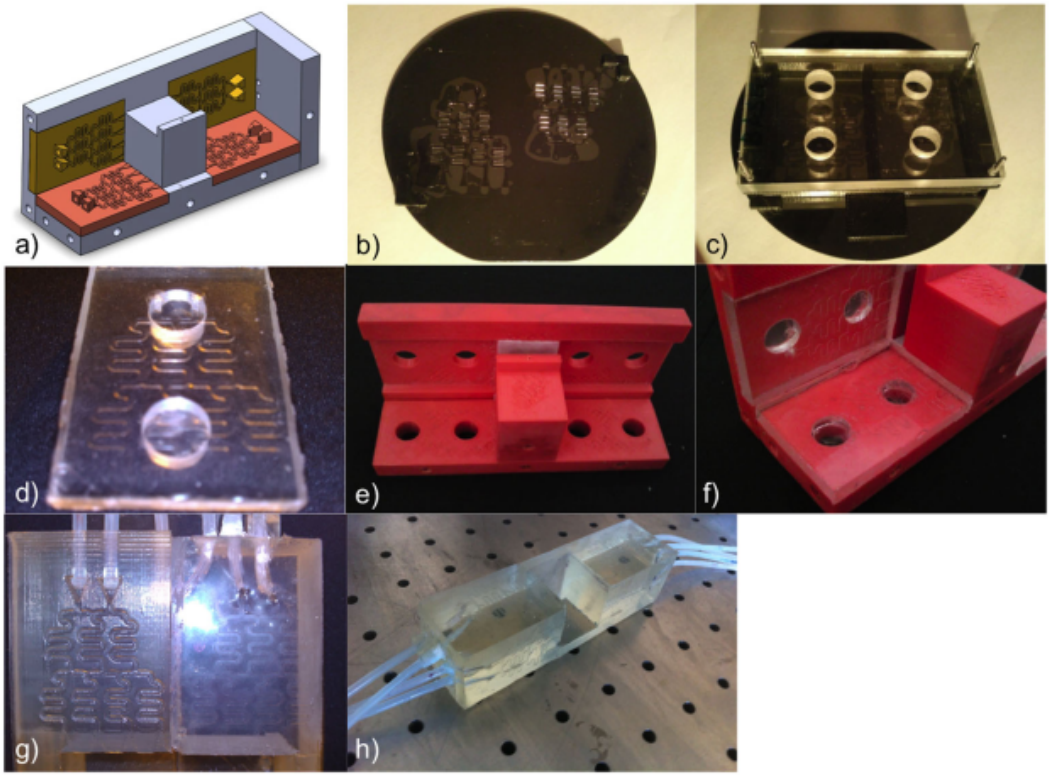

Figure 2. Steps towards the realization of the three-dimensional (3D) gradient maker (GM): (a) concept; (b) realization of SU-8 negative on the silicon wafer; (c) Plexiglas cover on silicon wafer, with holes for casting PDMS; (d) PDMS positive of microchannels; (e) 3D printed support; (f) assembly; (g) differences between PDMS cast on a 3D printed mould (on left) and the one made with our mould (right). The surface of the one on the right is flat, thus avoiding leakages; (h) view of the completed PDMS core.

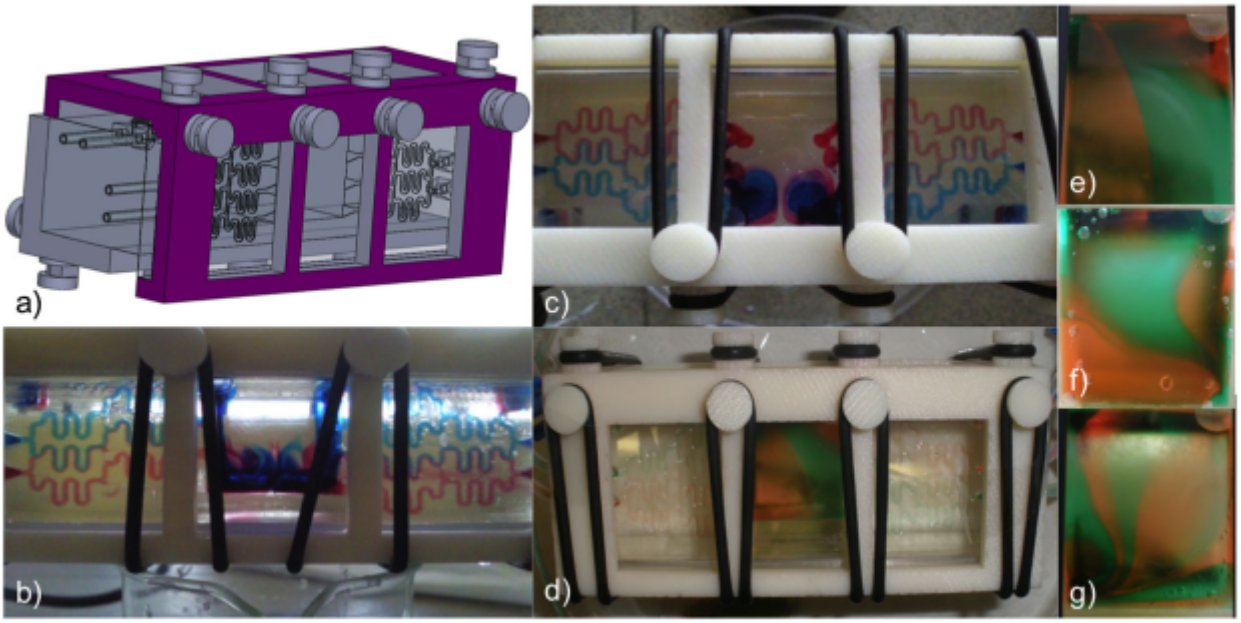

Figure 3. The three-dimensional (3D) gradient maker (GM) and its sealing system: (a) concept and design; (b) front and (c) top view of the assembled device with a dye gradient developing inside; (d) view of the assembled device with a gradient developed inside the chamber; (e–g) examples of the different gradients that could be developed by varying the flow rates and the distribution of dyes at the inlets.

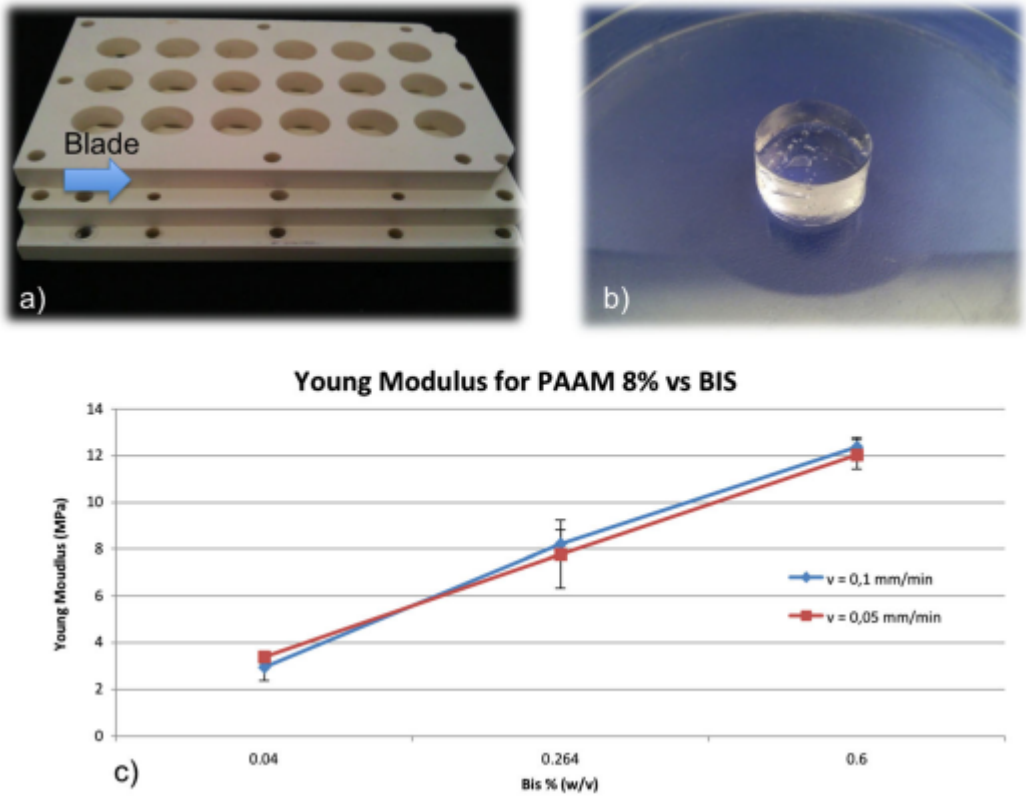

Figure 4. Mechanical characterization of polyacrylamide (PAAM) hydrogels as a function of bisacrylamide (BIS) concentration: (a) view of the support used for uniform testing samples making; (b) view of a 8% PAAM sample, its surfaces are both flat; (c) PAAM Young modulus vs. BIS concentration. It can be seen that neither of the deformation velocities (corresponding to 0.0125/min and 0.0063/min strain rates, respectively) affect the curve behaviour.

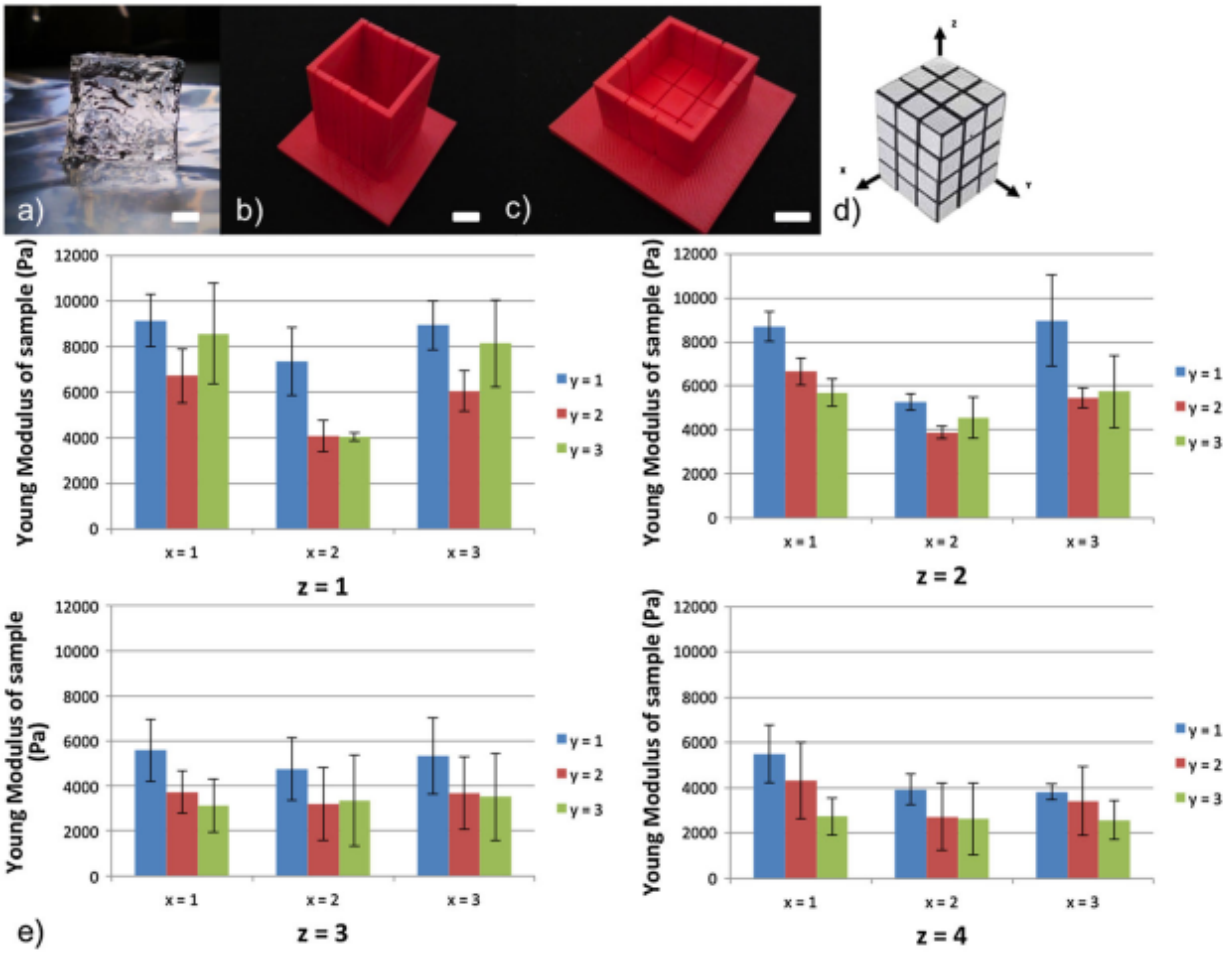

Figure 5. The polyacrylamide (PAAM) 'cube': (a) view of the polymerized PAAM cube inside the gradient maker (GM); (b) view of the first slicing tool (the blade passes between the spaces in the plastic, slicing the cube in four pieces); (c) view of the second slicing tool (the samples cut before are split in nine parts); (d) view of conceptual cube slicing; (e) Experimental measurements of stiffness distribution within the cube. A stiffness gradient can be seen in both z and y directions. Scale bars = 5 mm.

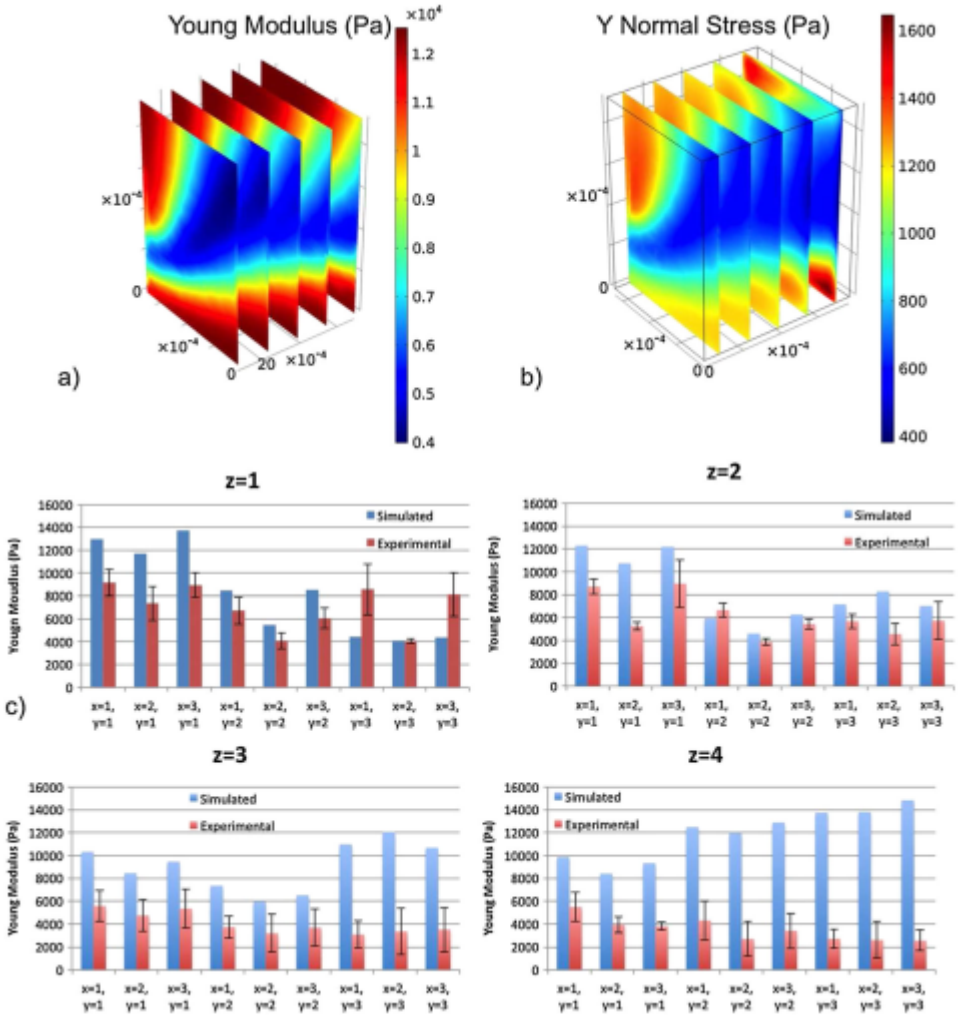

Figure 6. Finite element analysis simulation of sample stiffness: (a) Young modulus distribution (Pa) in a sliced part (x = 4, y = 2, z = 2); (b) stress distribution (Pa) in the 1% deformed sample; (c) experimental vs. simulated Young modulus. In the two upper slices (z = 1 and z = 2) there is not an exact matching, but the trends are, in general, close each other. The other slices show, instead, patterns different from those expected.